Methods

Treatment of $p53^{-/-}$ mice with R508 phosphorothioate antisense oligonucleotide.

Animal experiments were performed under approved IACUC protocol #11016 on eight-week old male C57BL/6J $p53^{-/-}$ mice on a B6.129S2-$Trp53^{tm1Tyj}$/J background purchased from Jackson Laboratory (Bar Harbor, ME). Mice with homozygous knockout of *RALBP1* (referred to here as $Rlip^{-/-}$) were generated by Lexicon genetics (The Woodlands, TX), and mice born of $Rlip^{+/-}$ x $Rlip^{+/-}$ mating, were genotyped by PCR strategy as described previously (1). R508 is based on the unique Rlip gene nucleotide sequence ^{508}GGCTCCTGAATTGGCTTTTTC^{529} with the least homology to nucleotide sequences in the human or mouse genome. Control scrambled phosphorothioate oligonucleotide (CAS) sequence, generated using GenScript software was CATCGAAATCGTTGCAGTTAC. CAS does not deplete Rlip or cause apoptosis, xenograft regression, hypoglycemia, hypolipidemia, or insulin sensitivity. R508 or CAS were dissolved in PBS (1 mg/mL) and 0.2 mL was administered weekly for by *i.p.* injection starting at 8 week age until euthanasia. Two sequential experiments were performed, with necropsy performed at 32 wk age in the first and 36 wk age in the second experiment.

Spontaneous and chemical carcinogenesis in p53 and Rlip knockout mice.

Cross breeding of $p53^{+/-}$ C57Bl6 mice with $Rlip^{+/-}$ was performed to obtain colonies of mice with the genotypes: $p53^{-/-}Rlip^{+/+}$, $p53^{-/-}Rlip^{+/-}$, $p53^{-/-}Rlip^{-/-}$, and $p53^{+/-}Rlip^{+/-}$. For spontaneous carcinogenesis, mice were monitored 3 times per week for distress or overt malignancy and all surviving mice were euthanized at age 48 wk. Chemical carcinogenesis was studied in 10-15 mice of each genotype per treatment group. Mice were administered 3 mg B[a]P in 0.1 ml corn-oil or corn oil alone by gavage at the age of 8 and 12 weeks.

Cell culture.

All malignant cell lines were purchased from ATCC except for the mouse Raji and human LCL

lymphoma cell lines, which were a gift from Prof. Stephen J. Forman, City of Hope, Duarte, CA. Mycoplasma testing was done using Universal Mycoplasma Detection kit. Malignant cells were grown in RPMI1640 medium and MEFs in DMEM containing 10% FBS and 1% penicillin/streptomycin at 37 ^{o}C in 5% CO_2. Cytotoxicity, signaling, and endocytosis studies were performed in serum free medium after washing cells in Hanks' PBS.

Analysis of cancer-signaling and cytokine pathways by Western blot.

The effect of CAS or R508 treatment on signaling proteins in mouse liver was determined using 28,000 x g supernatant fraction of a 10% homogenate. For Western blotting, ~ 50 µg protein loaded per lane was subjected to SDS-PAGE and transferred onto the nitrocellulose membrane. Horseradish peroxidase (HRP)-conjugated anti-mouse and anti-rabbit secondary antibodies and primary antibodies towards CDK2, CDK4, pJNK (T^{183} / Y^{185}), β-actin, GAPDH and pAMPK (T^{172}), pAKT (S^{473}), pRb (S^{780}), pP70S6K (T^{389}), pPI3K (Y^{458}), Bcl2, Bax, pmTOR (S^{2448}) and pP38-MAPK (T^{180} / Y^{182}) were purchased from Santa Cruz Biotechnology, Inc. Detection was done using chemiluminescence ECL kit (Amersham Life Sciences). β-actin was used as loading control and representative results from one of several experiments are shown.

RNA-Seq studies and validation of results by qRT-PCR.

RNA was extracted using the RNeasy mini kit from Qiagen (Valencia, CA) according to manufacturer instructions. RNA quality was assessed by microfluidic capillary electrophoresis using an Agilent 2100 Bioanalyzer with RNA 6000 Nano Chip kit from Agilent Technologies (Santa Clara, CA). Sequencing libraries were prepared with the Ribo-Zero Gold rRNA Removal kit from Illumina (San Diego, CA), and followed by KAPA Stranded RNA-seq Library Preparation Kit from Kapa Biosystems (Wilmington, MA) according to the manufacturer's protocol. Briefly, 500 ng of DNA free total RNA from each sample was used for ribosomal RNA removal; the resulting ribosomal depletion RNA was fragmented with divalent cations under elevated

temperature. First-strand cDNA synthesis produced single-stranded cDNA. After second-strand cDNA synthesis, the double-stranded cDNA underwent end repair, 3′ ends adenylation, and finally the barcoded adaptors (Illumina) were ligated to the cDNA fragments, and 10 cycles of PCR was performed to produce the final sequencing library. The libraries were validated with the Agilent Bioanalyzer with the DNA Hisensitivity Chip. Library templates were prepared for sequencing using cBot cluster generation system (Illumina) with HiSeq SR Cluster V4 Kit. The sequencing run was performed in the single read mode of 51 cycle using Illumina HiSeq 2500 platform with HiSeq SBS V4 Kits. Real-time analysis (RTA) 2.2.38 software was used to process the image analysis and base calling. Reads were aligned using Tophat v2.0 to mouse reference genome mm9 (2, 3). Expression level of RefSeq genes were counted and normalized using TMM method (4) and differential expression analysis was conducted using a linear model based on negative binomial distribution using "edgeR". RPKM (reads per kilobase per million mapped reads) = # of reads / (gene length/1000 * total number of reads/1,000,000). Analyses were performed by censoring the lowest expressed genes or using $\log_2$(RPKM+0.1) expression levels. To satisfy the criteria for differential expression, a *p* value <= 0.01, fold change >= 2, and RPKM>=1 in at least 2 samples was required. RNA-Seq results were confirmed using real-time quantitative PCR. cDNA using gene primers was performed on an ABI-7500 fast real-time PCR system using SYBR Green master mix. 1 µg of total RNA from liver was used to synthesize cDNA by reverse transcription using the RT kit (Applied Biosystems). To validate RNA-Seq results, qRT-PCR was conducted with primers, pre-validated from BioRad (PrimePCR, cat. 10025636) for the following genes: Cib3, Dlk1, Cyp4a32, Fzd10, Gpr3, Tff1, and Six3. The internal control primer sequences for ZZZ3 were AGACCATTGCTGTACTTGAGG and GGTATGGAAGCCCTATGTCAG. Reactions were conducted in triplicate for each biological replicate and data is expressed as $\log_2$ fold change in $p53^{-/-}$ CAS or R508-treated mice relative to wild-type using the comparative *Ct* method. RNA-Seq data was normalized using the above internal reference genes and linear regression was

used to determine correlation between RNA-Seq and qRT-PCR data. GO pathway terms were ranked by *p*-value (EASE score) (3-6).

Whole-genome bisulfite sequencing.

For the whole-genome bisulfite sequencing, 200ng of DNA was sonicated with Covaris (Woburn, MA) with the setting for getting DNA size peaking at 200bp (7). The fragmented DNA was end-repaired and A-tailed by using the NEB Next kit according to the manufacturer's instructions. Illumina's Methylated Adaptor was used for the adaptor ligation. The adaptor-ligated DNA was treated with EZ DNA methylation Gold kit from Zymo (Irvine, California) according to the manufacturer's instructions. Bisulfite-treated DNA was amplified using PfuTurbo Cx Hotstart DNA Polymerase from Agilent Technologies with 10 cycles of PCR. 1.0xAmpure beads from AGENCOURT (Brea, CA) were used for the PCR products purification. Library templates were prepared for sequencing using cBot cluster generation system (Illumina) with HiSeq PE Cluster V4 Kit. Sequencing run was performed in the paired end mode of 101cycle using Illumina HiSeq 2500 platform with HiSeq SBS V4 Kits. Real-time analysis (RTA) 2.2.38 software was used to process the image analysis and base calling.

Reads were aligned to in silico bisulfite converted mm9 genome using Bismark aligner (8) using default settings. The methylation level of each CpG site was calculated as the number of non-converted cytosine divided by the sum of converted and non-converted cytosine. CpG sites with less than 3x coverage were excluded. Methylated regions were defined as those with $\geq$ 5 pairs of CpG sites merged if they were <200-bp apart. Those with $p \leq 0.05$ and average difference $\geq$ 0.25 were considered significant. To determine the methylation levels of CpG sites within promoters, we used the RefSeq gene's promoter region (defined as $\pm$ 1000 bp of transcription start site) to calculate average promoter methylation level. Promoters having at least one sample with > 50% methylation level and range of methylation level across the four samples > 25% were selected for analyses. To identify the regions that were hyper-methylated

in sample A vs. B (differential methylated regions), the regions had to satisfy three criteria: 1) methylation level in sample A was > 60%; 2) methylation level in sample B was < 50%; and 3) the methylation difference was > 45%. DMRs were annotated using the mm9 RefSeq database. Regions between 1kb from transcription start site to transcription end site were categorized as “gene body”; regions not overlapping with above regions were categorized as “intergenic”.

Quantitative validation was carried out for the PTPN6 and HOXA5 gene promoters by conventional bisulfite sequencing. Bisulfite conversion of genomic DNA was performed with EpiTect Bisulfite Kit (Qiagen). Primers were designed with MethPrimer software using genomic coordinates of identified regions of differential methylation (9). The forward/reverse primer sequences were as follows: PTPN6- ATTTAAGGTGGATGATGGTGTTATT/ TCCAAAACTCAAAAAACTTCTATAACC; HOXA5 - GTTTGATGATTTTTAGAGGTAAATT/ CCATAATAAACTATAACCTCAATTC; corresponding annealing temperatures were 53 and 52 ^{o}C. Bisulfite PCR-amplified DNA was separated using 2% agarose gel electrophoresis and bands extracted with a Gel Extraction Kit (Qiagen). Purified target DNA was cloned into pDrive vector and EZ competent cells were transformed with plasmid DNA (PCR Cloning plus Kit; Qiagen). DNA was isolated from transformed bacteria (Qiaprep Spin Miniprep; Qiagen) and sequenced at City of Hope DNA sequencing core. Finally, DNA methylated sequence analysis was conducted with Bisulfite Sequencing DNA Methylation Analysis Software v9 (BISMA).

Statistical Analyses.

Statistical methods used for RNA-Seq, WGBS and expression array analyses are given above. Results for both types of studies were analyzed for effects on genes, pathways and processes using Integrated Pathways Analysis (IPA, Qiagen Inc.) and DAVIDv6.7 (Database for Annotation, Visualization and Integrated Discovery).GOTERM_BP_FAT, GOTERM_CC_FAT, GOTERM_MF_FAT, and KEGG_PATHWAY databases were included. Enriched ontology

terms had to have >4 genes and an EASE score <0.05. Ontology results from each database were ranked by p-value. For analyses of DMRs lists, the genomic region had to exceed >100 identifiers. For other studies, experimental group comparisons were performed using two-tailed unpaired student's *t* test are expressed as the mean ± SD. The statistical significance of differences between control and treatment groups was determined by ANOVA followed by Bonferroni correction and Benjamini-Hochberg procedure with false discovery rate <0.05. Changes in tumor size and body weight during the experiments were visualized by scatter plot. Differences were considered statistically significant if $p<0.05$. All scalar data were evaluated with two-tailed paired or unpaired Student's *t* test and comparisons of three or more groups were compared by one-way ANOVA. Results and are expressed as the mean ± SD. A value of $p<0.05$ was considered statistically significant.

References for Supplemental Material

1. Awasthi S*, et al.* (2005) RLIP76 is a major determinant of radiation sensitivity. *Cancer research* 65(14):6022-6028.
2. Li H, Ruan J, & Durbin R (2008) Mapping short DNA sequencing reads and calling variants using mapping quality scores. *Genome Res* 18(11):1851-1858.
3. Li R, Li Y, Kristiansen K, & Wang J (2008) SOAP: short oligonucleotide alignment program. *Bioinformatics (Oxford, England)* 24(5):713-714.
4. Zhou Y, Lin N, & Zhang B (2014) An iteration normalization and test method for differential expression analysis of RNA-seq data. *BioData mining* 7:15.
5. Huang da W, Sherman BT, & Lempicki RA (2009) Systematic and integrative analysis of large gene lists using DAVID bioinformatics resources. *Nature protocols* 4(1):44-57.
6. Zhao S, Fung-Leung WP, Bittner A, Ngo K, & Liu X (2014) Comparison of RNA-Seq and microarray in transcriptome profiling of activated T cells. *PloS one* 9(1):e78644.
7. Hahn MA LA, Wu X, Pfeifer GP (Cancer Epigenetics. *In: Methods in Molecular Biology book series*), pp pp 273-287.
8. Krueger F & Andrews SR (2011) Bismark: a flexible aligner and methylation caller for Bisulfite-Seq applications. *Bioinformatics (Oxford, England)* 27(11):1571-1572.
9. Li LC & Dahiya R (2002) MethPrimer: designing primers for methylation PCRs. *Bioinformatics (Oxford, England)* 18(11):1427-1431.

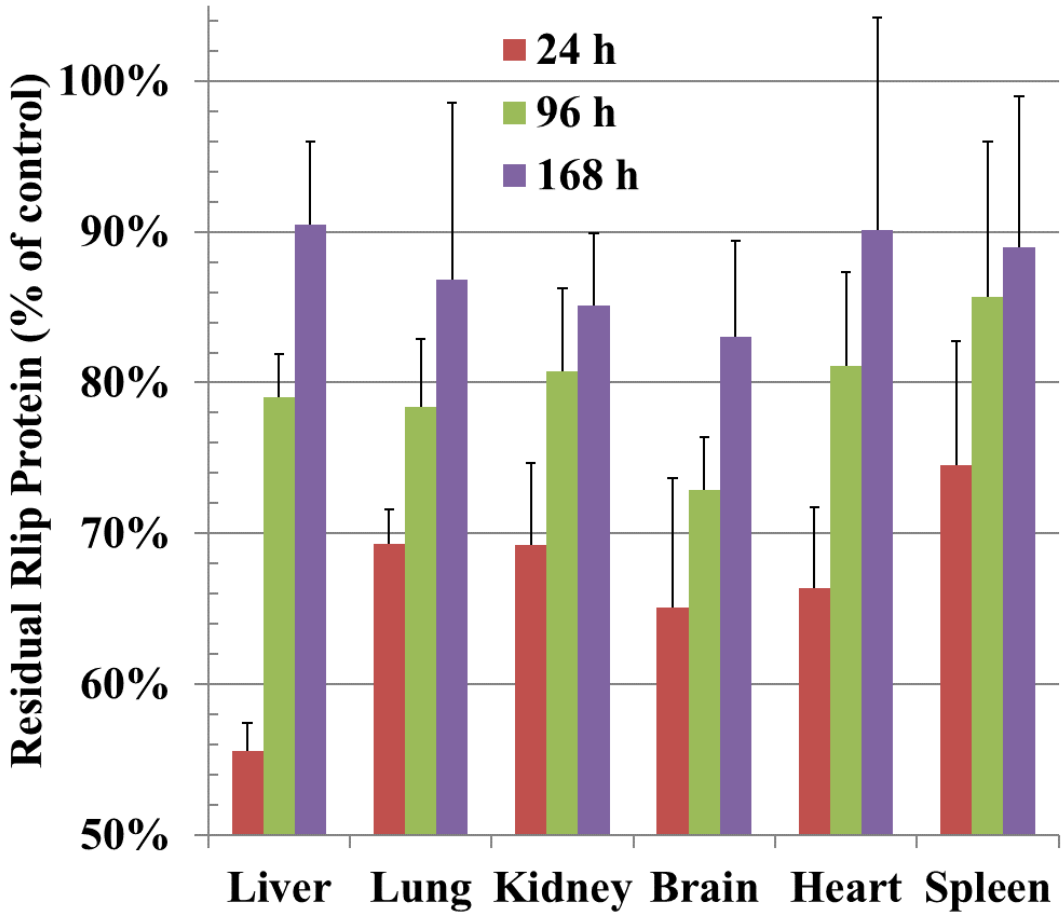

Suppl. Fig. 1 Rlip depletion by R508 in tissues of WT mice

12-week old WT C57BL-6 mice treated with R508 (200 µg/0.2 mL, i.p.) and euthanized at 24, 96 and 168 h (3 mice/time point). The 28,000 x g supernatant of crude membrane fraction of liver, lung, kidney, brain, heart and spleen tissue was assayed by an ELISA assay using anti-Rlip antibodies from Santa Cruz Biotechnology (Columbus, OH).

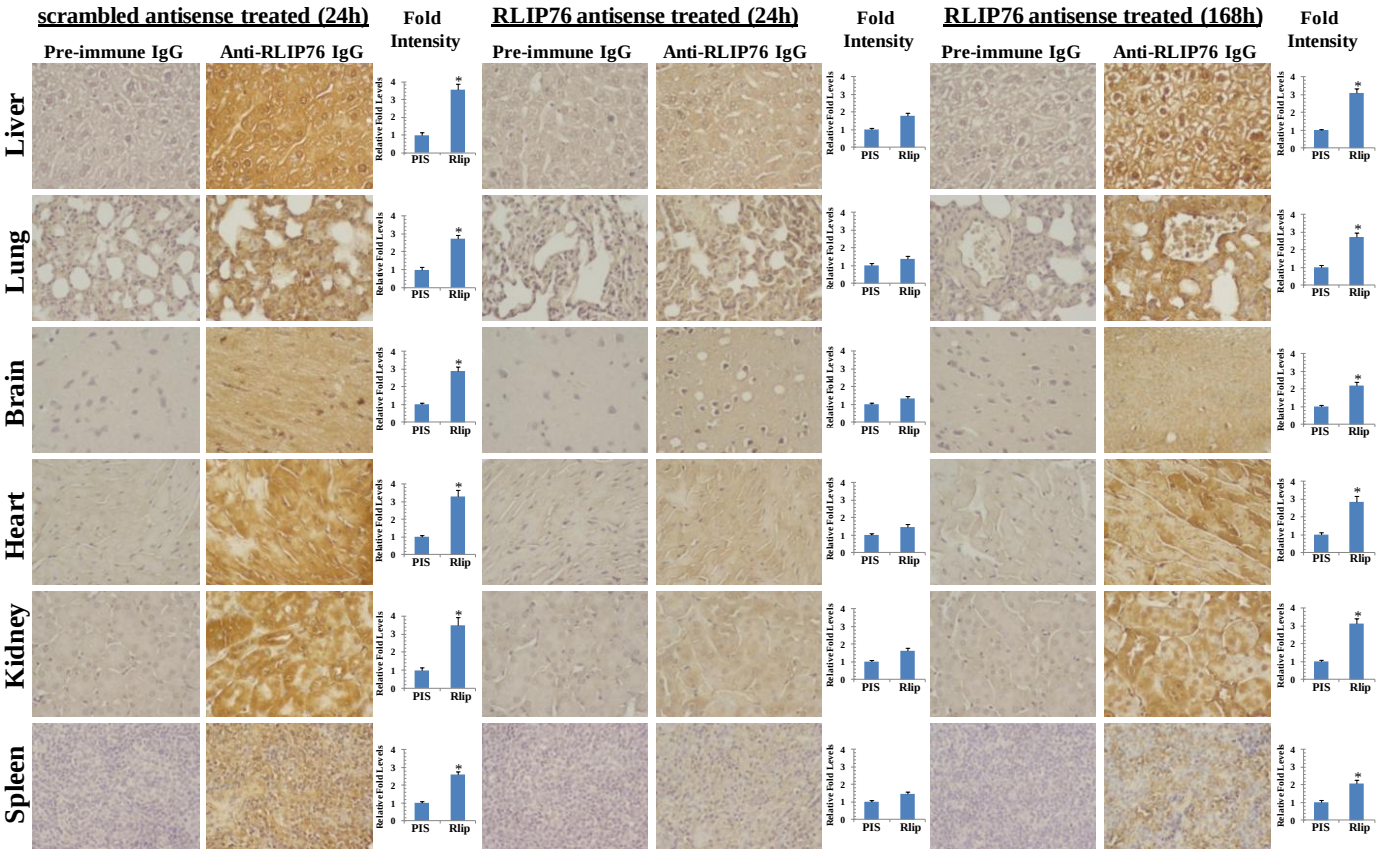

Suppl. Fig. 2 Rlip protein in tissues of R508-treated wild-type mice by immunohistochemistry

12-week old WT C57BL-6 mice treated with R508 or CAS (200 µg/0.2 mL, i.p.). 5 µm thick histological sections of formalin-B5 fixed tissues were subjected to IHC assays with polyclonal rabbit anti-human Rlip (Alpha Diagnostics, San Antonio, TX) primary and HRP-conjugated goat-anti-rabbit (Santa Cruz Biotechnology) secondary antibodies. Universal ABC detection kit (Vector) was used for staining. Microscopic analyses and photomicrography were performed using an Olympus DP2 microscope interfaced with DP2-BSW software and Image Pro plus 6.3 software (Media Cybernetics Inc., Bethesda, MD) by veterinary pathologist blinded to the treatment groups.

Results shown above are from IHC with pre-immune or anti-Rlip antibodies for CAS-treated mice euthanized at 24 h (left columns), R508-treated mice euthanized at 24 h (middle columns) and R508-treated mice euthanized at 168 h. Relative staining intensity of photomicrographs (20x objective) is shown to the right in blue bars. Statistical significance (shown as * for $p<0.001$) is from 2-sided *t-tests*.

Rlip protein was depleted in all tissues by R508 maximally by 24 h with recovery by 168 h. Maximum depletion was in the liver. The results were concordant with ELISA assays for rlip protein in liver homogenates.

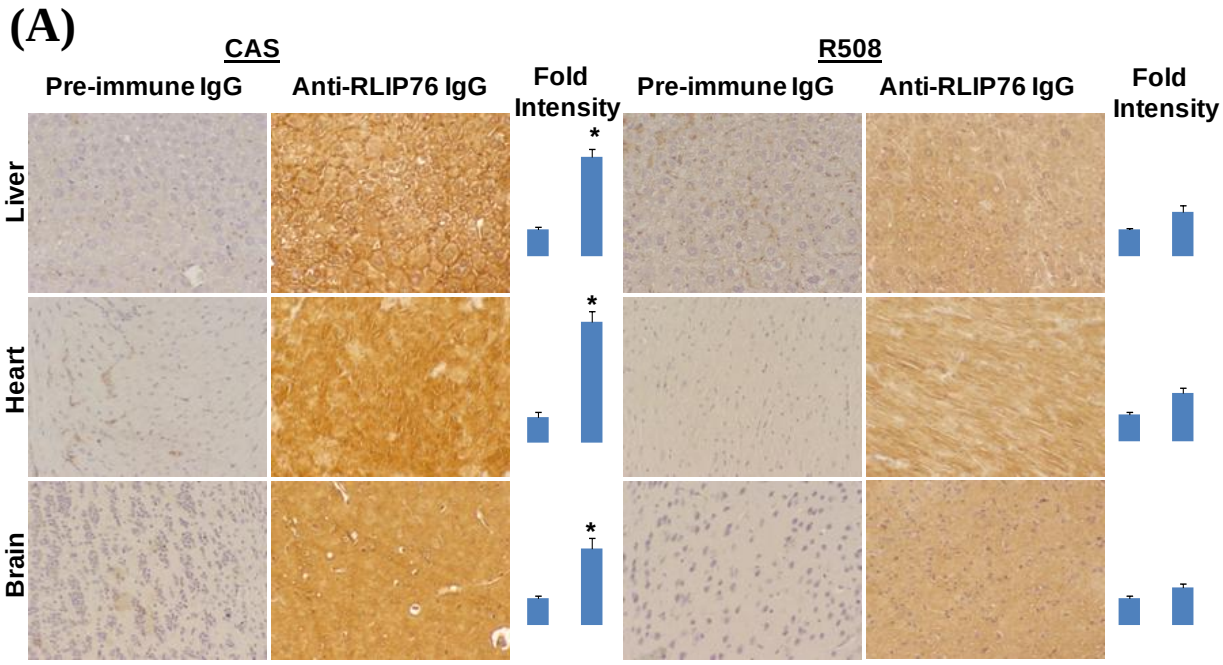

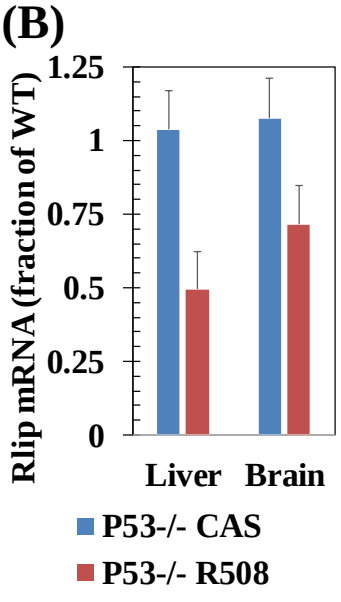

Suppl. Fig. 3. Rlip depletion by R508 in p53$^{-/-}$ mice treated with R508

(A) Results of IHC using either pre-immune or rabbit-anti-human Rlip antibody is shown for liver, heart and brain tissue sections from CAS and R508 treated mice, with relative staining intensity shown in blue bars to the right of photomicrographs. **(B)** Rlip mRNA was determined by real-time qRT-PCR in the liver and brain tissue of CAS (scrambled antisense) or R508 (Rlip-directed antisense) treated mice by procedures described in *Methods*.

Pre-immune IgG showed no staining; anti-Rlip IgG revealed reduction of Rlip protein in R508 treated liver, heart and brain tissues. Rlip mRNA was depleted to approximately half of control upon R508 treatment. Rlip mRNA in brain tissue was also lowered, but to a lesser extent.

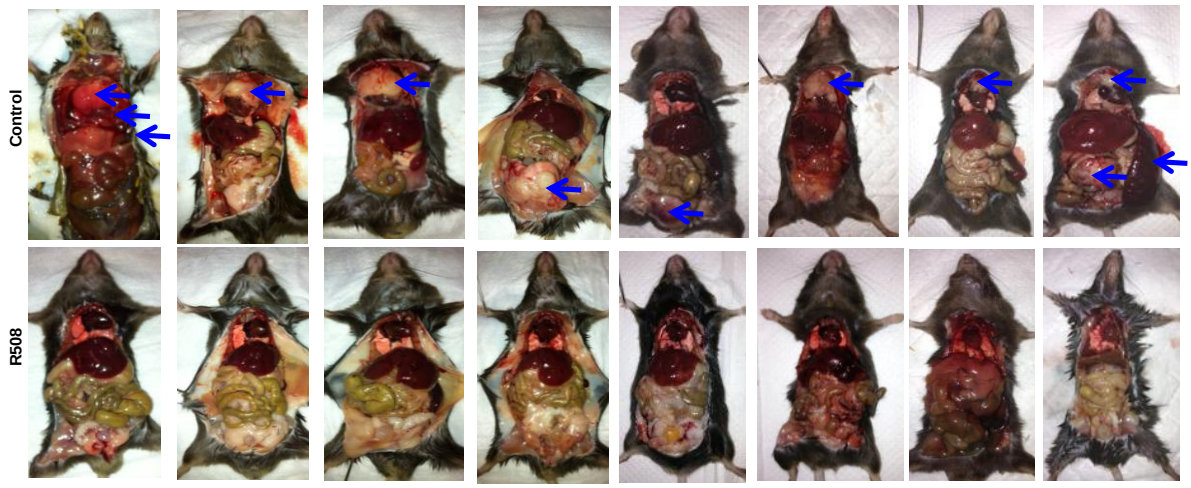

Suppl. Fig. 4 Necropsy of R508 and CAS treated p53$^{-/-}$ mice.

Animal experiments were performed under approved IACUC protocol #11016. Eight week old male C57BL/6J p53$^{-/-}$ mice on a (B6.129S2-Trp53tm1Tyj/J) background were purchased from Jackson Laboratory (Bar Harbor, ME). p53-/- mice were divided into two groups (control and experimental) of 8 animals in each group. All mice were treated beginning at age 8-weeks with weekly *i.p.* injection of 0.2 mL PBS containing CAS (control) or R508 (0.2 mg/0.2 mL) for 24 weeks with twice daily inspection. Euthanasia was performed in morbid mice and all surviving animals were euthanized at 32 wk age in the first and 36 wk age in the second experiment. Complete gross and microscopic necropsy analyses were performed in the ARC animal pathology using Olympus DP2 microscope with DP2-BSW software and Image Pro plus 6.3 software (Media Cybernetics Inc, Bethesda, MD).

The masses seen in the control animals were excised, weighed, fixed in formalin-B5 fixative, sectioned and used for H&E staining as well as immunohistochemistry. **Blue arrows** point to masses in the mediastinum and testes. 7/8 R508 mice survived without tumor at 32 wk. One R508-treated mouse (lower row, last column) was euthanized due to inanition at 28 wk age, but had no tumor.

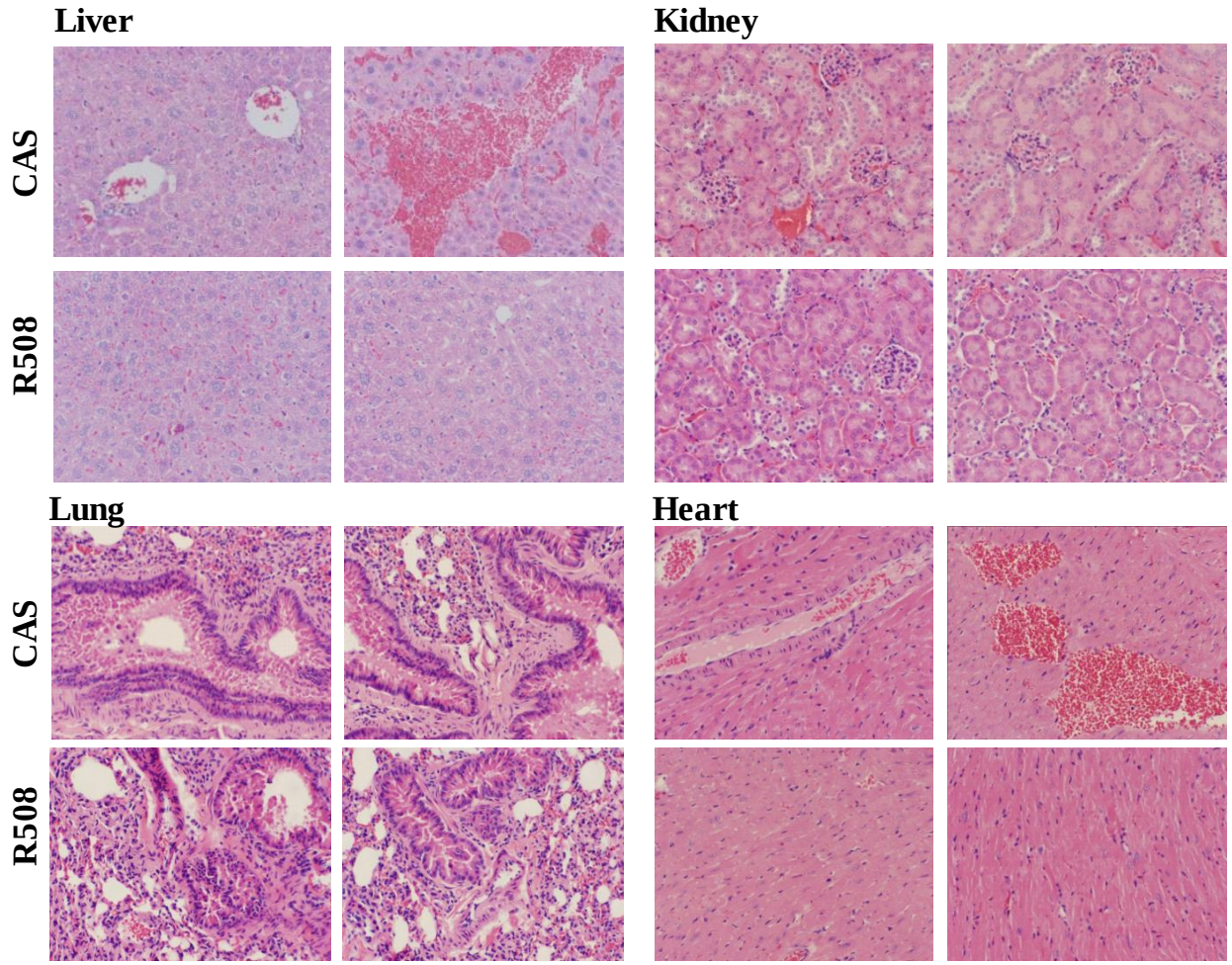

Suppl. Fig. 5. Histology of tissues grossly uninvolved with lymphoma

Histological sections of H&E-stained tissues grossly uninvolved with tumor masses from CAS or R508 treated mice are shown. Hemorrhagic areas involving the liver, kidney and heart tissues were observed in the CAS-treated mice whereas tissues from R508-treated mice were histologically normal. Lung tissues were relatively unaffected in both groups.

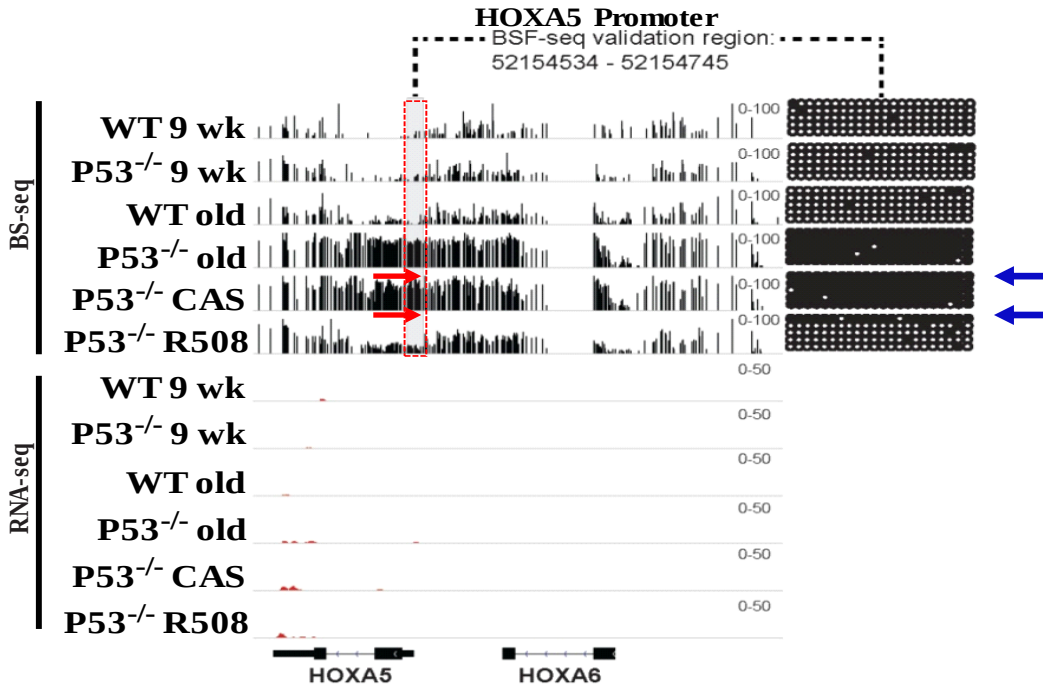

Supp. Fig. 6. Validation of WGBS by conventional bisulfite sequencing of the HOXA5 promoter and alignment of WGBS and RNA-Seq results

Bisulfite conversion of genomic DNA was performed with EpiTect Bisulfite Kit (Qiagen). Primers for bisulfite PCR as well as optimal PCR conditions were designed with MethPrimer software using genomic coordinates of identified regions of differential methylation. Bisulfite PCR-amplified DNA was electrophoretically separated on 2% agarose gel and bands extracted with a Gel Extraction Kit (Qiagen). Purified target DNA was cloned into pDrive vector and EZ competent cells were transformed with plasmid DNA (PCR Cloning plus Kit; Qiagen). DNA was isolated from transformed bacteria (Qiaprep Spin Miniprep; Qiagen) and sequenced. DNA methylation sequence analysis was conducted with Bisulfite Sequencing DNA Methylation Analysis (BISMA) software 9 (http://bmcbioinformatics.biomedcentral.com/articles/ - 10.1186/1471-2105-11-230). Sequences from WGBS and RNASeq were aligned as described in *Methods* and visualized using IGV viewer.

The treatment groups are indicated on the left for each row in each panel. The top six rows are from WGBS with black bars representing quantitative DNA methylation and the bottom six rows are the corresponding aligned RNASeq results with red bars representing number of reads. The gray row below shows the location of exons (vertical black lines) and introns. Red boxes highlight regions with DMRs reverted towards wt by R508 treatments. The grid shown on the right represents the results of conventional bisulfite-seq (CBS) on the promoter region highlighted by the gray box. Each grid is aligned with the treatment group shown on the left. Dark spots represent hypermethylated areas and white spots are unmethylated regions.

The results showed that the hypermethylated regions found by WGBS (red arrows) in the control $p53^{-/-}$ mice were also hypermethylated by CBS (blue arrows), validating WGBS results.

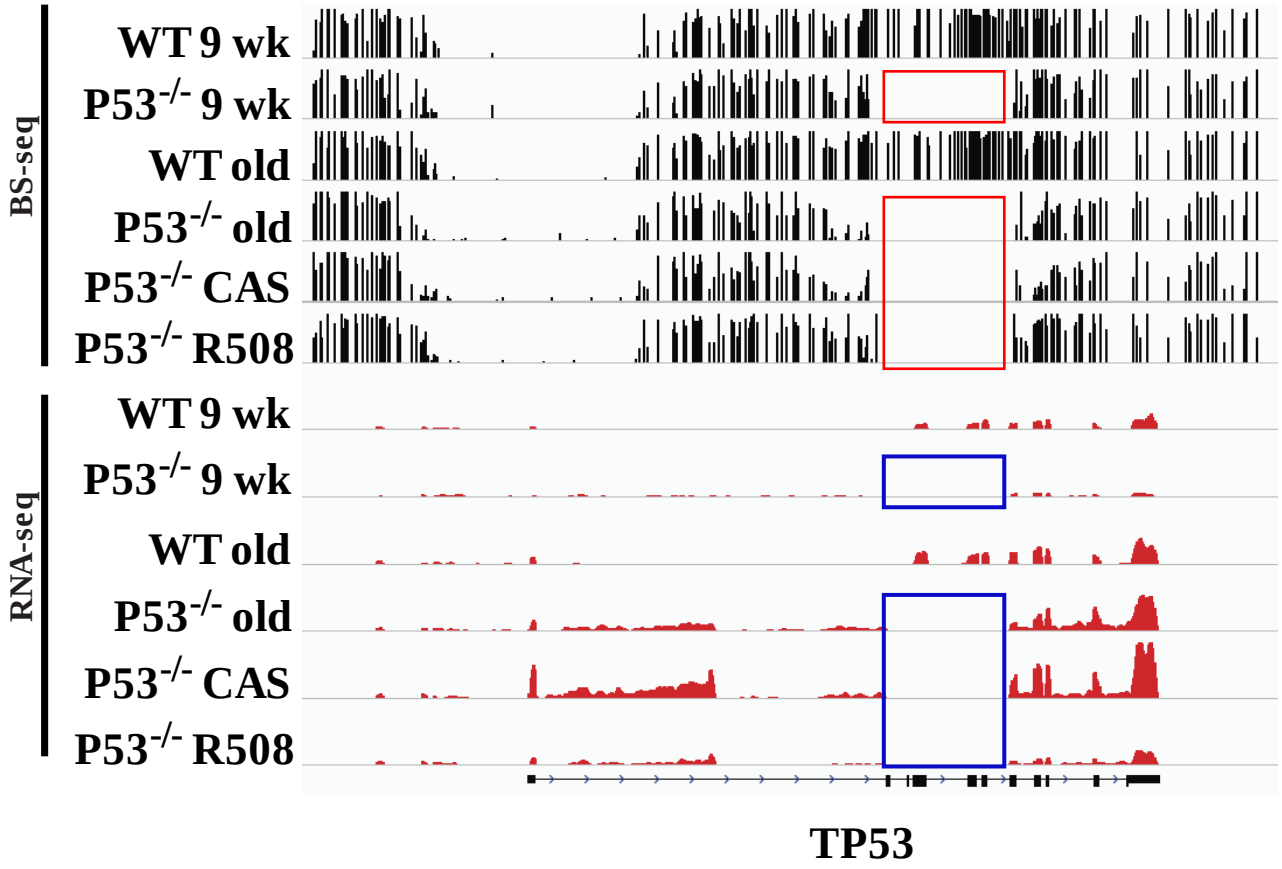

Suppl. Fig. 7 Aligned RNA-Seq and bisulfite-Seq sequence of the p53 gene

RNA-seq, whole-genome bisulfite sequencing and sequence alignment were performed as described in Methods. Sequences from WGBS and RNA-seq were visualized using IgV viewer. The experimental groups were: *wt* young and p53$^{-/-}$ young (9 week old), *wt* old (32 week old), PBS-p53$^{-/-}$ (PBS-treated p53$^{-/-}$ mouse 20 week old at death), CAS-p53$^{-/-}$ ((PBS-treated p53$^{-/-}$ mouse 22 week old at death), and R508-p53$^{-/-}$ (R508-treated p53$^{-/-}$ mouse 32 week old at euthanasia). Aligned sequence reads in RNA-Seq are shown below the WGBS data (top). Red bars are proportional to expression.

The genotype of p53$^{-/-}$ was confirmed by the absence of reads corresponding to the p53 gene in WGBS DNA (red boxes) aligned with RNASeq results (blue boxes). Interestingly, despite lacking essential p53 exons in p53$^{-/-}$ mice, the p53 promoter becomes hypomethylated and this is reversed in R508-treated p53$^{-/-}$ mice (red box).

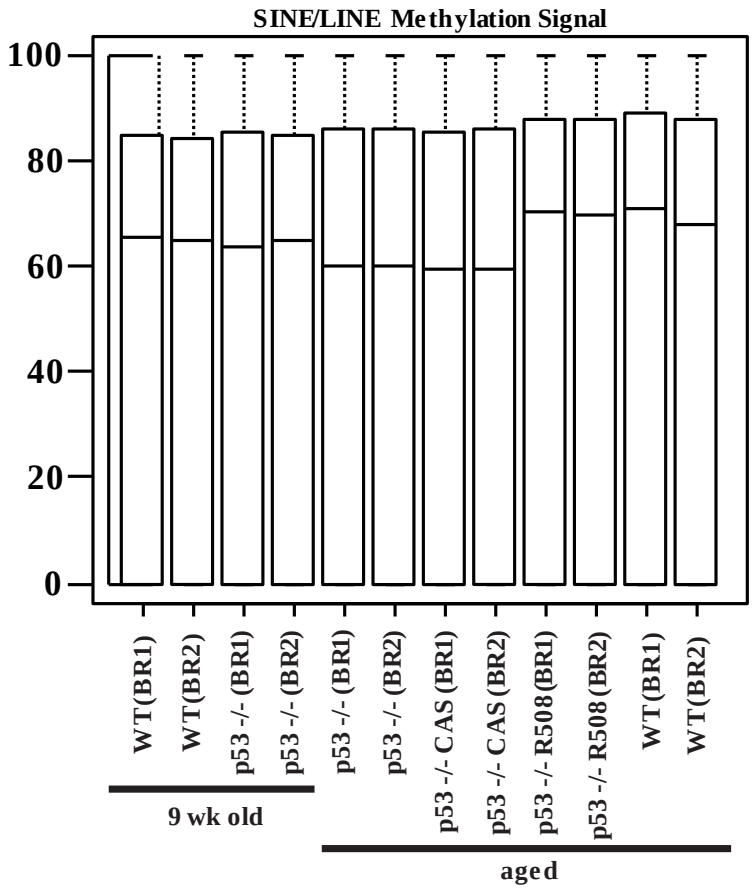

Suppl. Fig. 8A Sine/Line Methylation Signals

A. Sine/Line element methylation. WGBS sequencing was performed as described in *Methods*. mm9 SINE/LINE elements were downloaded from RepeatMasker track at UCSC genome browser. The methylation level at each SINE/LINE element was the average methylation level of all CpG sites falling into the element. Bars display median. BR1 and BR2 are biological replicates.

Results show reduced median methylation of SINE/LINE elements in untreated and CAS-treated $p53^{-/-}$ mice that reverts towards wild-type with R508 treatment. In addition, we observed that young $p53^{-/-}$ had quantitative Sine/Line methylation levels similar to 32 week *wt* mouse.

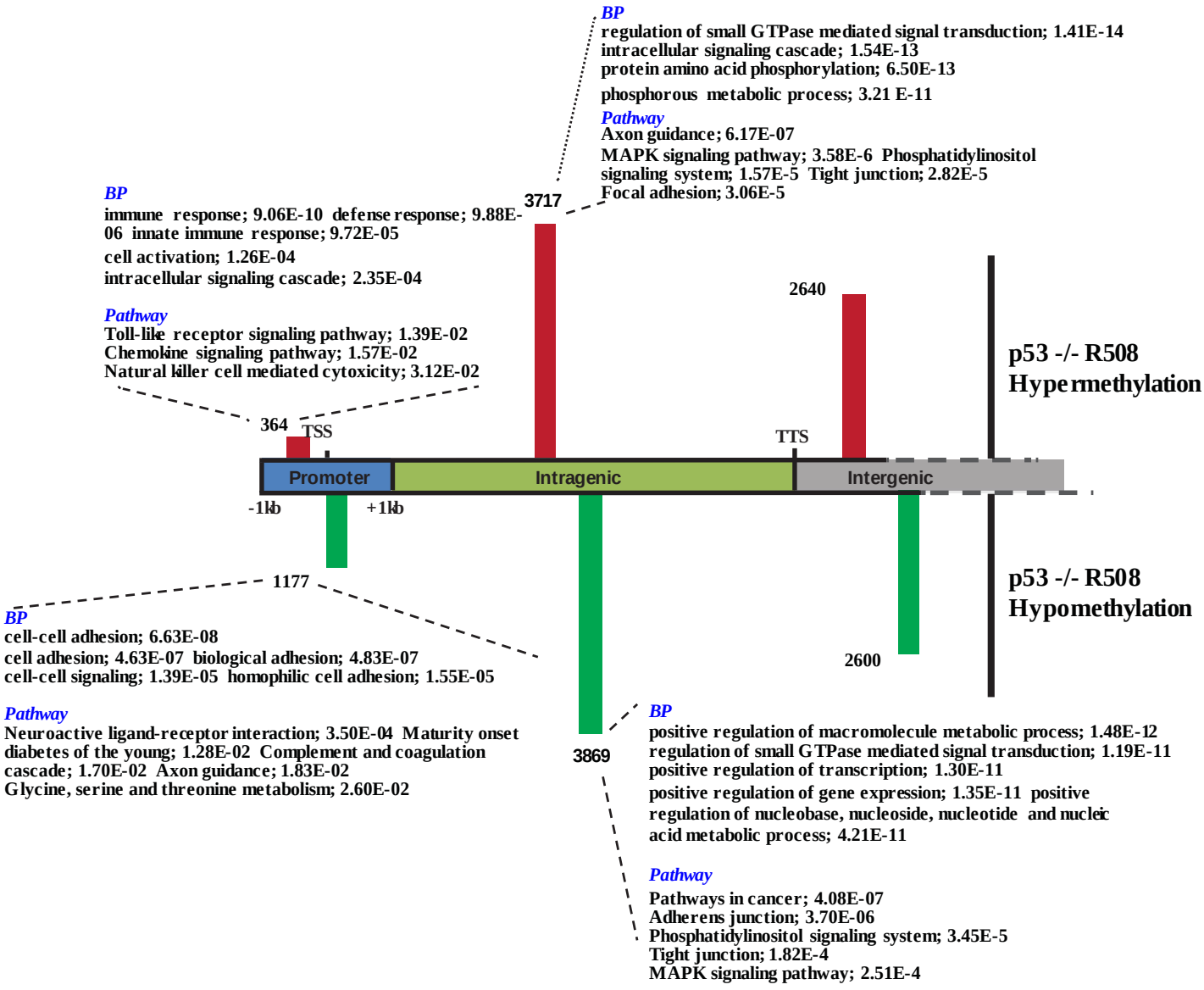

Suppl. Fig. 8B. Quantification of DMRs by genomic region bisulfite sequencing The Database for Annotation, Visualization and Integrated Discovery (DAVID) v6.7 was utilized for gene ontology analysis with the following constraints: 1) DMR lists by genomic region must exceed >100 identifiers 2) GOTERM_BP_FAT, GOTERM_CC_FAT, GOTERM_MF_FAT, and KEGG_PATHWAY databases were included 3) and enriched ontology terms included >4 genes and had an EASE score <0.05. Ontology results from each database were ranked by p-value. Quantification of DMRs by genomic region was compared between CAS vs. R508-treated p53 -/- mice. Red bars=hypermethylated DMRs; green bars=hypomethylated DMRs. The top 5 biological process (BP) or KEGG Pathway enriched terms are displayed for DMRs as indicated.

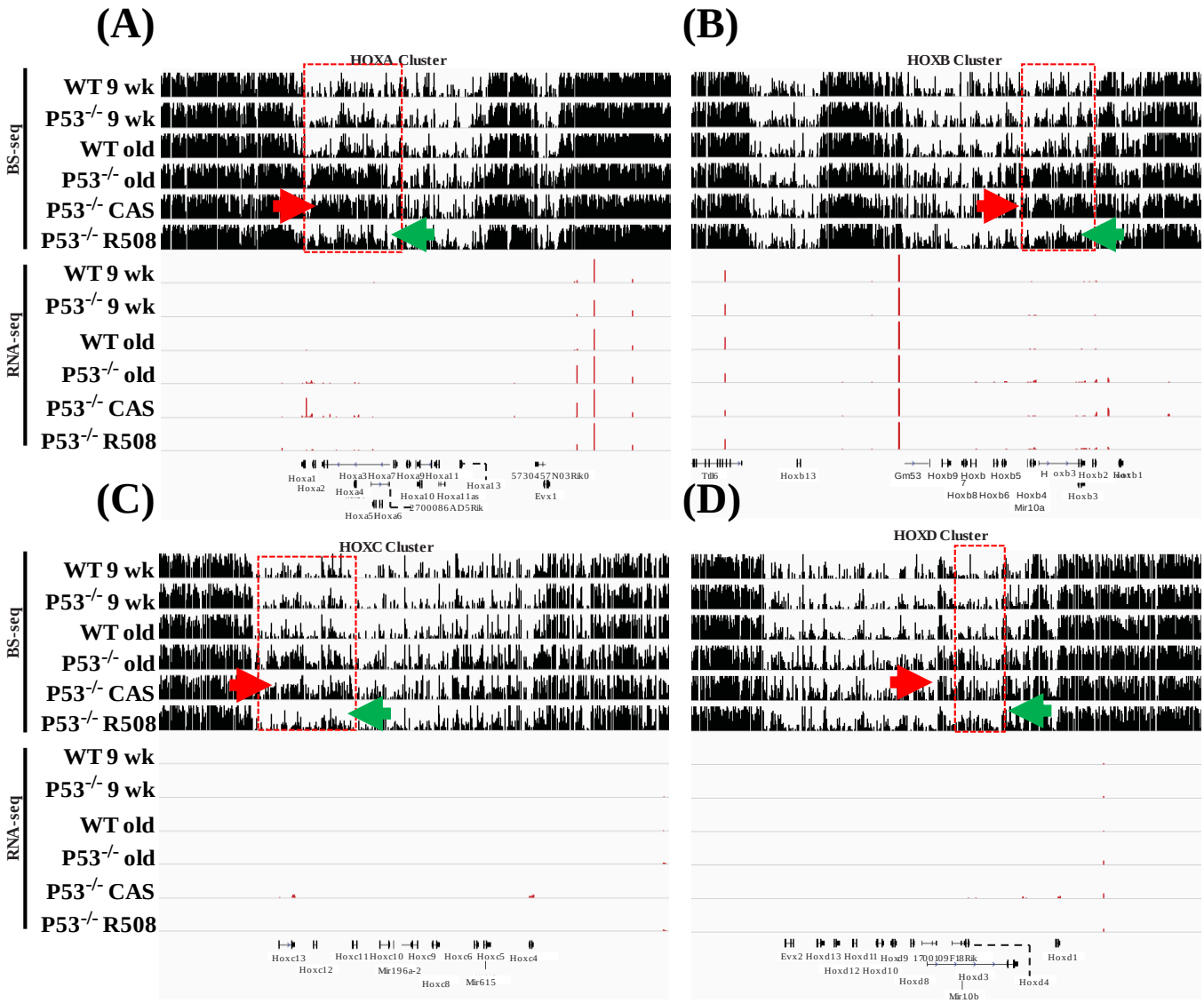

Suppl. Fig. 9. Differential methylation of promoter and gene bodies aligned with RNA-Seq results of HOX A, B, C and D cluster genes

RNA-seq, whole-genome bisulfite sequencing and sequence alignment were performed as described in Methods. Sequences from WGBS and RNA-seq were visualized using IgV viewer. The treatment groups are indicated on the left for each row in each panel. The top six rows are from WGBS with black bars representing quantitative DNA methylation and the bottom six rows are the corresponding aligned RNASeq results with red bars representing number of reads. The gray row below shows the location of exons (vertical black lines) and introns.

Results for (**A**) HOXA, (**B**) HOXB, (**C**) HOXC and (**D**) HOXD are shown with red boxes highlighting regions with hypermethylated promoter DMRs (red arrows) in control p53$^{-/-}$ mice reverted towards *wt* by R508 treatments (green arrows).

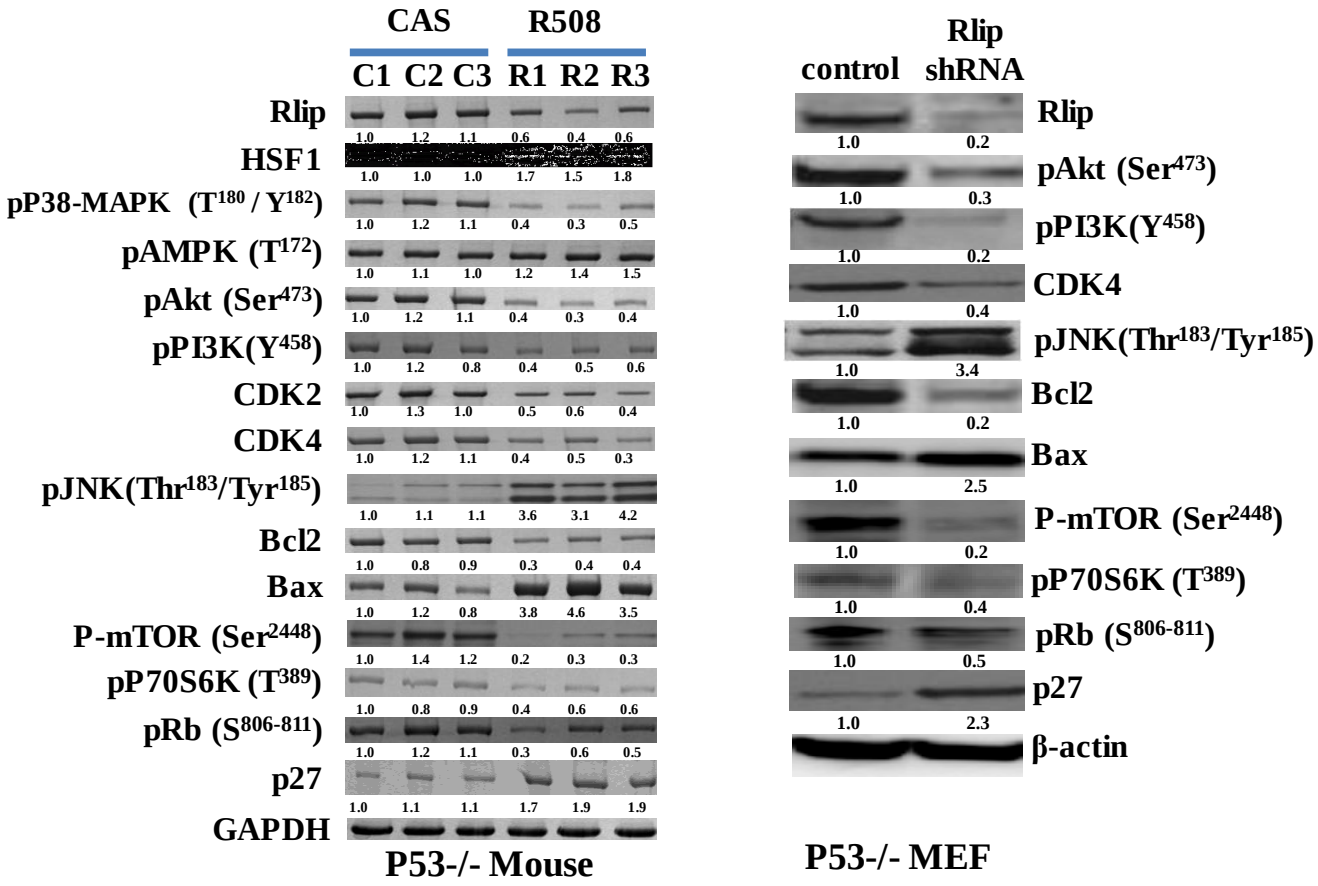

Suppl. Fig. 10. Effects of Rlip depletion on signaling proteins in p53-/- in mouse liver and MEF.

(A) The effect of R508 treatment on signaling proteins in mouse liver was determined using 28,000 x g supernatant fraction of a 10% homogenate. Results from studies performed on liver tissues from three biological replicates. C1-3 are from 3 CAS-treated mice and R1-3 are from 3 R508-treated mice. **(B)** The effect of Rlip-depletion on signaling in $p53^{-/-}$ MEF was determined by transfecting Rlip and corresponding scrambled shRNA (pSR/puro plasmids, Addgene, Cambridge, MA) using lipofectamine 2000 (Invitrogen) followed 24 h later by lysis. Western blotting was performed as described in the Methods section of the manuscript. Density of bands was quantified using an Alpha Imager. MEFs were derived and maintained in culture at 12 to 13-day gestation by previously described methods (26). $P53^{-/-}$ MEFs were provided by Dr. Arnold J. Levine, Cancer Institute of New Jersey/UMDNJ, New Brunswick, NJ.

Multiple cancer promoting pathways were affected by R508. In general, cell proliferation and growth pathways were increased while apoptosis pathways were decreased. The effects of Rlip depletion by shRNA in $p53^{-/-}$ MEF largely reflected those seen in the liver tissues of mice, indicating that the effects observed were specific for Rlip deficiency.

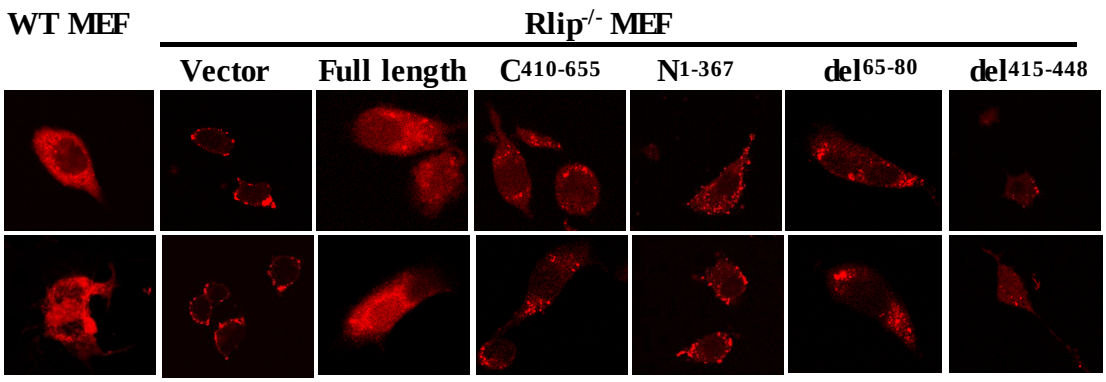

Suppl. Fig. 11. Restoration of endocytosis of EGF in Rlip$^{-/-}$ MEF by wild type versus transport deficient mutants of Rlip.

Endocytosis of EGF in Rlip$^{-/-}$ MEF transfected with wild type full length as well as transport deficient mutants. Transport deficient mutants were prepared as follows. DNA encoding the N-terminal fragment (N^{1-367}) was amplified by PCR (up-stream primer 5'-GGCCTCGAGATGACTGAGTGCTTC-3‘ containing the underlined Xho I site; downstream primer 5'-AGAGCGGCCGCCTAGAGTTCTT GCACATGTGT-3‘, containing the underlined Not I site). The purified fragment was cloned into pGEM-T plasmid and cut with Xho I. The cohesive ends blunted with Klenow DNA polymerase and dNTP were then cut with Not I, and the resulting fragment was subcloned into pET-30c(+). DNA encoding the C-terminal fragment ($C^{410-655}$) was amplified by PCR (up-stream primer 5'-AGCCATATGCACCACCACCACCACCACAATTGTTTACATCG AGAT-3' with the underlined Nde-I restriction site; down-stream primer 5'-GCACTCGAGTCAGATGGACGTCTCCTTCCT-3' with underlined Xho I restriction site) and subcloned into pET-30b(+). For the $del^{415-448}$ we used 5’ GAATTGTTTACATCGACAGGAGTGTGAAACC (with its reverse complement), and for del^{65-80} 5’GTGTCTGATGATAGGACTGAAGGCTATG 3’ and its reverse complement.

Rlip$^{-/-}$ or Rlip$^{+/+}$ MEFs (0.1 x 10^6 cells/mL) were grown on sterilized glass cover slips in RPMI 1640 medium followed by washing with Hanks buffer. Then the cells were incubated with 100 µL of rhodamine red conjugated EGF (40 ng/ml prepared in DMEM medium containing 1 % BSA) for 60 min at 4 ^{o}C followed by incubation at 37 ^{o}C in humidified chamber for 10 min. The cells were then fixed with 4 % paraformaldehyde. The cover slips were mounted on slides upside down with Vectashield mounting medium. The Slides were analyzed using confocal laser scanning microscopy with Zeiss 510-meta system at 40x magnification with excitation wave length at 488 nm and emission 580 nm. Two representative example slides are shown for each.

Rlip$^{-/-}$ MEF had markedly decreased endocytosis as compared with *wt* and the vector transfection did not replace this, but full length Rlip cDNA restored endocytosis. The C-terminal, N-terminal and ATP-binding-site-deletion mutants were less effective and resulted in different patterns of vesicle trafficking. Transport activity of Rlip is necessary for normal CDE function.

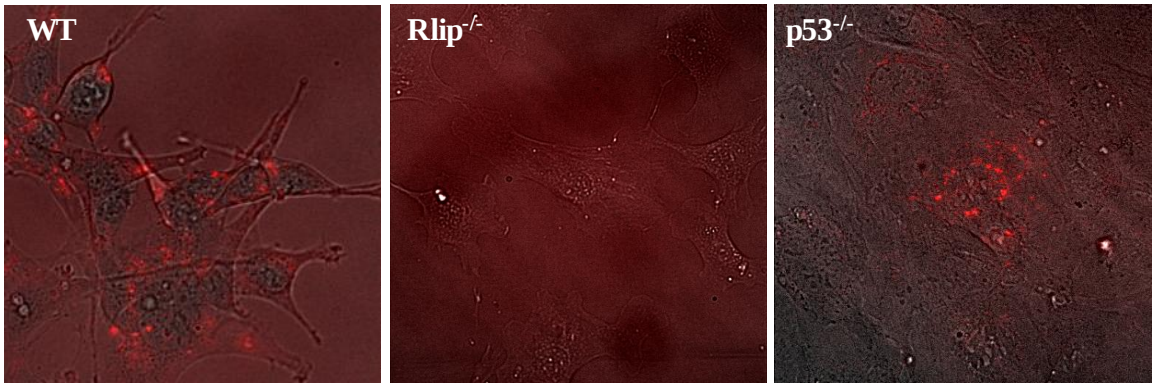

Suppl. Fig. 12. Endocytosis of EGF in Rlip$^{-/-}$ and p53$^{-/-}$ MEF

Rhodamine-EGF was prepared using a molar ratio of 6:1::NHS-rhodamine (in DMSO at 10 mg/mL): antibody (1 mg/mL in PBS/1% BSA, pH 7.2). After incubation on ice at 2h, excess NHS-rhodamine was removed using a Dye Removal Column from Thermo Scientific (cat# 22858). Live cells were grown attached to sterilized cover-slips followed by addition of rhodamine-EGF. The Zeiss LSM 880 Confocal fluorescence microscope with Airyscan technology and ZEN imaging software was used to capture images of live cells at 2 min intervals for 30 min.

The results confirmed the marked deficiency of endocytosis in Rlip$^{-/-}$ MEF (26). In addition, endocytosis was also impaired in p53$^{-/-}$ MEF.

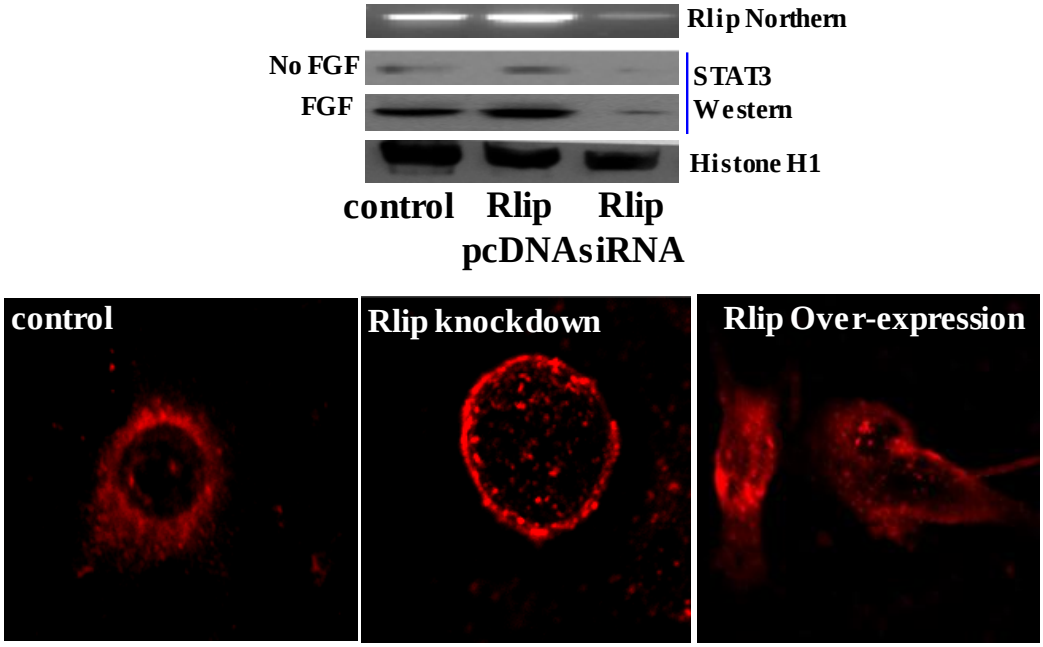

Suppl. Fig. 13. Regulation of FGF endocytosis and signaling by Rlip in B-16 melanoma

(A) To determine if Rlip regulates STAT3 signaling down-stream of FGF Rlip was over-expressed using an Rlip-pcDNA3.1 plasmid containing full-length recombinant human Rlip cDNA or knocked down using Rlip siRNA. mRNA was amplified by RT-PCR and Northern blot was used to confirm over-expression or knockdown. Forward and reverse primers used for qRT-PCR were: nt 334-353 (5' TTCAAGAAGCCCAGCTTTTC) and nt 812-831 (5' ATTCTCTGGAAGGTCTCGCA), respectively. At 48 h after transfection, cells were serum starved for 6h, then treated with 50 ng/mL recombinant murine FGF (Peprotech, Rocky Hill, NJ). The effect of over-expression or down-regulation or Rlip on FGF signaling was examined by measuring STAT3 translocation into nucleus. Nuclear extracts were prepared using the Epigentek nuclear extraction kit. The extract was subjected to SDS-PAGE and Western blotting against polyclonal full-length rabbit-anti-human IgG. Histone-H1 was the internal loading control. Results for cells treated without or with FGF are presented, showing untransfected control, Rlip-over-expressing, and Rlip knockdown cells. **(B)** For studying the role of Rlip in regulating FGF endocytosis, Quantum-dot labeled FGF (QD605-FGF) complexes were prepared by incubating 8 µM Qdot ITK Amino (PEG) in 0.25 mL 50 mM borate pH 8.3 containing 1 mM Bis[sulfosuccinimidyl] suberate for 30 min at 20 ^{o}C, purified using a NAP-5 desalting column (Amersham Biosciences) in PBS at pH 7.4,and functionalized with FGF by incubating for 2 h with 50 µg human FGF. After quenching with 50 mM glycine the conjugate was purified by ultra-filtration on a 100 kDa filter. Adherent melanoma cells growing on sterile glass slides were treated with QD^{605}-FGF on ice in DMEM medium for 45 min at 4 ^{o}C, washed with PBS, and incubated for 0 and 10 min in PBS at 37 ^{o}C. Slides were fixed in 4% paraformaldehyde and cover slips were mounted on slides upside down with Vectashield mounting medium and analyzed using confocal laser scanning microscopy with Zeiss 510-meta system, with excitation at 594 nm and emission 610 nm.

In B16 melanoma cells, FGF-induced STAT3 signaling was activated by Rlip over-expression and inhibited by Rlip depletion. This correlated with increased endocytosis of FGF upon Rlip over-expression and reduced endocytosis upon rlip depletion.

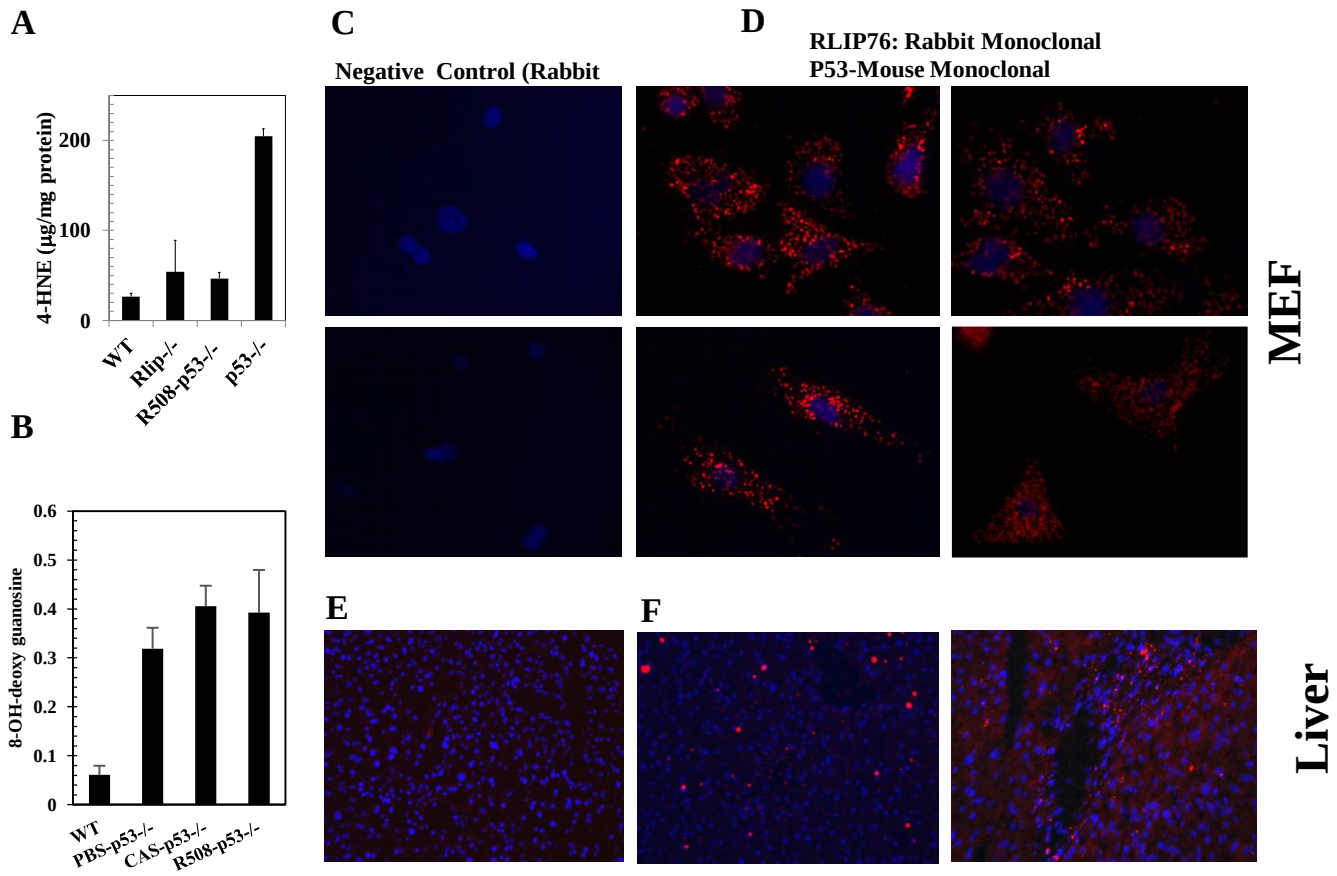

Suppl. Fig 14. Effect of R508 on oxidative stress damage and stress-responses.
(A) The 4-hydroxynonenal (4HNE) and (B) 8-OH-deoxyguanosine (8OHdG) levels were measured in liver homogenate using Oxiselect kits from Cell Biolabs, San Diego, CA. A 96-well plate ELISA assay was used with spectrophotometric detection using a Tecan Pro200 plate reader at 450 nm. Analyte concentrations were estimated using standards provided in the respective kits. (C, F) Interactions between Rlip, p53 and HSF1 in wt MEF and liver tissue sections were studied by proximity ligation assays (PLA, Duolink® In Situ Orange Starter Kit Mouse/Rabbit, Sigma, St. Louis MO) in (C, D) cultured wt MEFs and (E, F) 5 µm liver tissue sections. Primary anti-HSF1 rabbit monoclonal antibody (D3L8I) and anti-p53 mouse monoclonal antibody was from Cell Signaling Technology (Danvers, MA) and rabbit monoclonal anti-Rlip antibody was from Abcam (Cambridge, MA). The corresponding probes for PLA were anti-rabbit PLUS and anti-mouse MINUS antibody probes provided in the kit and used according to the manufacturer's instructions. In (C) Rlip antibody was omitted in the control shown for MEF studies; additional controls, where either p53 antibody or secondary antibody were omitted, are not shown. In (E) the control with p53 antibody omitted is shown for tissue studies; additional controls are not shown. (F) Results of interaction of HSF1 with p53 and (F) Rlip with p53 in mouse liver tissue are shown. Slides were visualized by fluorescence microscopy using an Olympus BX50 microscope (40x objective)

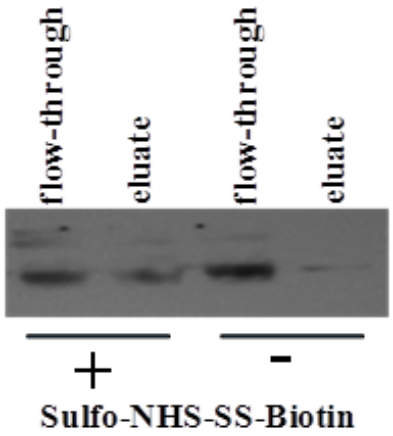

Suppl. Fig 15. Presence of the Rlip1$^{71-185}$ epitope on the cell surface of B16 melanoma cells

Presence of the Rlip$^{171-185}$ peptide epitope on the cell surface of B16 melanoma cells was determined using Thermo Scientific Cell Surface Protein Isolation Kit which is based on alkylation of cell surface peptides using the cell impermeable sulfo-NHS-SS-biotin reagent followed by isolation and solubilization of the membrane fraction as described in Methods. The membrane fraction was passed over an avidin affinity column and the flow-through fraction was collected. The bound fraction was eluted with biotin according to the manufacturer's instructions. The flow-through and eluent fractions were subjected to Western blot analyses using the rabbit-anti-human antibody against the Rlip171-185 peptide. The plus (+) and minus (-) symbols designate cells treated with or without Sulfo-NHS-SS-Biotin reagent.

The results showed enrichment of Rlip protein in the eluted fraction of Sulfo-NHS-SS-Biotin treated cells (second lane from left), indicating presence of this epitope on the cell surface.

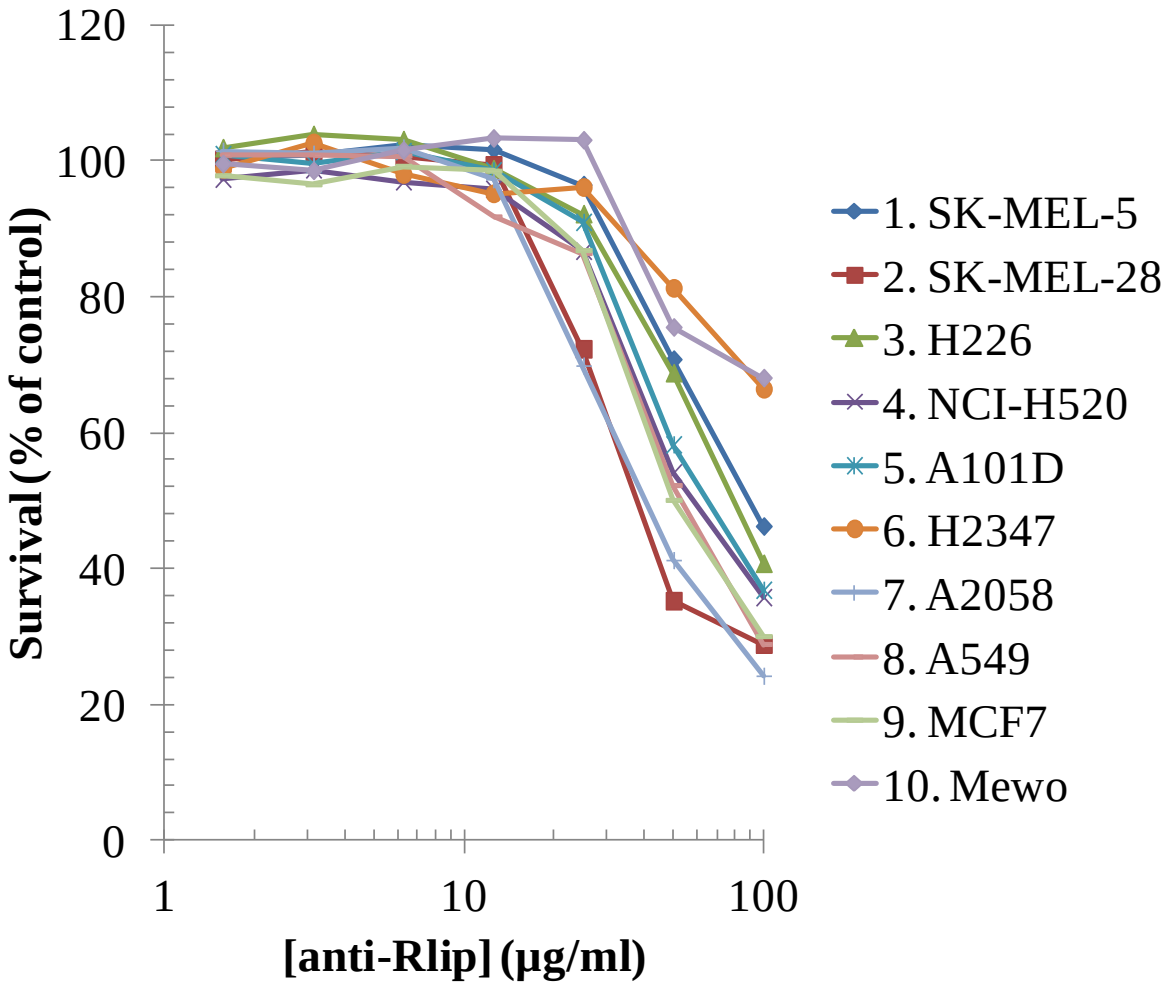

Suppl. Fig. 16. Growth inhibition by anti-Rlip$^{171-185}$ antibody in multiple malignant cell lines. Growth inhibition curves showing the concentration dependent effects of the anti-Rlip$^{171-185}$ antibody against multiple malignant cell lines: melanoma, (SK-MEL-5, SL-MEL-28, A101D, A2058 and MeWo), human NSCLC (H226, H520, H2347, and A549) and human breast (MCF7) is shown. Results are from one of three experiments, with 8 technical replicates.

Control

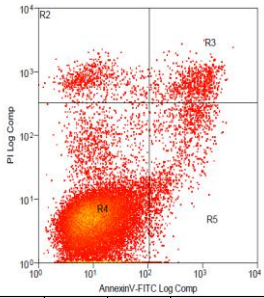

Region	Count	% Hist	Median
Total	28457	100	10.85; 4.90
R2	673	2.36	8.73; 742.32
R3	846	2.97	769.62; 642.46
R4	25770	90.56	10.09; 4.56
R5	1168	4.1	279.94; 35.72

Anti-Rlip Ab$^{171\text{-}185}$ (10µg/ml)

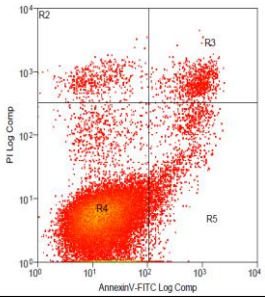

Region	Count	% Hist	Median
Total	28658	100	16.14; 5.27
R2	511	1.78	10.09; 742.32
R3	830	2.9	14.48; 666.08
R4	25855	90.22	14.48; 4.90
R5	1462	5.1	2225.39; 22.34

Anti-Rlip Ab$^{171\text{-}185}$ (20µg/ml)

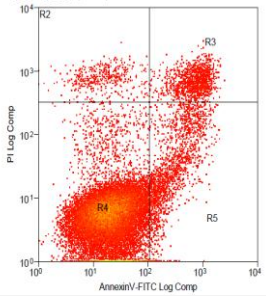

Region	Count	% Hist	Median
Total	28403	100	22.34; 5.87
R2	444	1.56	14.48; 769.62
R3	1342	4.72	769.62; 642.46
R4	24650	86.79	19.33; 5.27
R5	1967	6.93	225.39; 21.54

Anti-Rlip Ab$^{171\text{-}185}$ (40µg/ml)

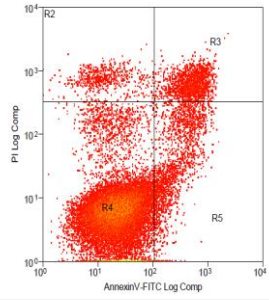

Region	Count	% Hist	Median
Total	27222	100	25.81; 6.78
R2	676	2.48	12.09; 742.32
R3	1956	7.19	536.31; 597.68
R4	22483	82.59	21.54; 5.66
R5	2107	7.74	217.40; 23.76

Suppl. Fig. 17. Apoptosis and necrosis induced by anti-Rlip$^{171\text{-}185}$ antibody in lymphoma cell lines

Apoptosis and necrosis induced in Raji mouse lymphoma cells by anti-Rlip$^{171\text{-}185}$ (10, 20 or 40 µg/mL) at 24 h after treatment was determined by flow cytometry using annexin V and propidium iodide staining according to procedures described in Methods. The fractions of apoptotic as well as necrotic cells at each concentration of antibody are shown in the tables.

The results demonstrated that anti-Rlip$^{171\text{-}185}$ antibody increased the apoptotic fractions (upper right quadrant) and the necrotic fraction (lower right quadrant) indicating that targeting this epitope of Rlip at the cell surface kills lymphoma cells.